Validation of the Use of Synthetic Near-Fault Ground Motions to Estimate the Response of a Concrete Building in a Risk Assessment Framework

Mayssa Dabaghi
Visiting Assistant Professor, Dept. of Civil and Environmental Engineering, American University of Beirut, Beirut, Lebanon

Panagiotis H. Galanis,
Postdoctoral Researcher, ETH, Zurich, Switzerland

Armen Der Kiureghian
Professor, Dept. of Civil Engineering, UC Berkeley, Berkeley, CA, USA

Jack P. Moehle
Professor, Dept. of Civil Engineering, UC Berkeley, Berkeley, CA, USA

ABSTRACT: In this study, the incremental dynamic analysis method or IDA (Vamvatsikos and Cornell, 2002) is used in the collapse performance evaluation of a reinforced concrete building subjected to near-fault ground motions. The analysis is performed for two sets of ground motions: (1) a recorded dataset based on FEMA P695 (2009); and (2) a synthetic dataset corresponding to the recorded one and generated using the parameterized stochastic model of near-fault ground motion by Dabaghi and Der Kiureghian (2014). The results show that the synthetic dataset tends to slightly underestimate the collapse capacity of the studied building compared to the recorded dataset. Despite this fact, the study demonstrates the potential of using synthetic ground motions in future applications of performance-based earthquake engineering.

1. INTRODUCTION

In recent years, seismic risk assessment of older non-ductile reinforced concrete buildings has become a top priority for seismic safety legislation in seismic-prone regions like California. The conservatism related with the current seismic policy often leads to unrealistically high costs of seismic retrofit. Recent advances in computational tools and performance based earthquake engineering have facilitated more realistic evaluation of risk using non-linear dynamic analyses.

A common method of evaluating the collapse performance of a structure is Incremental Dynamic Analysis (IDA) (Vamvatsikos and Cornell, 2002), whereby very strong recorded ground motions are gradually scaled until the structure reaches collapse. Since intense ground motions that significantly contribute to the seismic risk are infrequent and scarcely recorded, substantial upward scaling of the recorded motions may be necessary, and may yield scaled time series that are unrealistic. Alternatively, very strong synthetic ground motions may be used in addition to or in place of recorded ones. The use of synthetic ground motions is not common practice in IDA, but is particularly suitable when cloud analysis is used in place of IDA to evaluate collapse performance. In cloud analysis, the non-linear dynamic analysis of a structure is performed using a set of unscaled ground motions (e.g., Baker, 2007b).

This paper does not go as far as using synthetic ground motions in a cloud analysis

procedure. It simply compares IDA results from recorded and simulated ground motions as a validation exercise for the simulated motions. The validated simulated motions may later be used in a cloud analysis. In this study, the building whose collapse risk is evaluated using IDA is a fictitious 6-story reinforced concrete building with seismic detailing following the ACI 318-11 provisions; the study may later be extended to older non-ductile buildings that lack proper earthquake detailing.

The study focuses on near-fault ground motions, which may exhibit a large velocity pulse due to forward directivity. This near-fault effect often occurs when the fault rupture propagates towards the site with a velocity almost equal to the shear-wave velocity, and may impose a large demand on structures (Somerville et al. 1997). IDA is performed for two sets of pulse-like near-fault ground motions: (1) a recorded dataset based on FEMA P695 (2009); and (2) a synthetic dataset corresponding to the recorded one and generated using the parameterized stochastic model of near-fault ground motion by Dabaghi and Der Kiureghian (2014).

First, the building assessed in this paper is introduced, and a model of it is developed that accounts for non-linear geometry and non-linear material properties. Then, the procedures used to select the dataset of recorded ground motions and simulate the dataset of synthetic ground motions are presented. Finally, IDA is performed on the recorded and simulated datasets and the collapse assessment results for the two datasets are compared and contrasted.

2. DESCRITPION AND DESIGN OF THE STUDIED BUILDING

The building assessed in this study is a fictitious 6-story, 5-bay reinforced concrete frame building developed for the purposes of the ATC 78 project (FEMA 2013; 2014); see Figure 1. This idealized building consists of four perimeter moment-resisting frames, two in each direction, designed to resist gravity and earthquake forces, and of interior frames designed to resist only gravity loads. Each perimeter frame was proportioned to have design strength sufficient to resist base shear of approximately 10% of half of the self-weight of the building.

The building was designed to satisfy the detailing and proportioning provisions of ACI 318-11 (2011), including all requirement for configuration and spacing of transverse reinforcement, all requirements for development and splicing of reinforcement and the requirement that the sum of nominal moment strength of columns be at least 6/5 times the sum of nominal moment strength of beams at every beam-column connection except for those located at roof level.

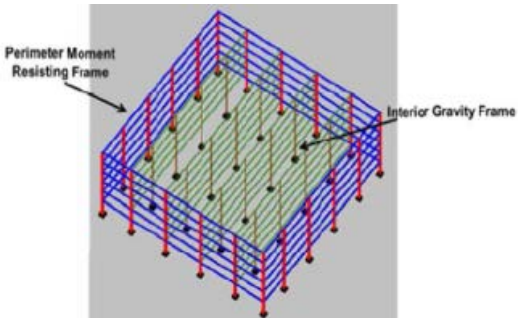

Figure 1: 3D view of the studied building

3. DEVELOPMENT OF NON-LINEAR MODEL FOR COLLAPSE SIMULATION

The studied building has a symmetric plan and thus responds to earthquake ground shaking with minimal plan torsion. Furthermore, the perimeter frames were assumed to provide the majority of resistance to lateral forces. Therefore, to simplify the analysis, the building was modeled using the two-dimensional (2D) frame shown in Figure 2 and that simulates only the vertical and lateral resistance of the perimeter frames. The perimeter frames in each direction were assumed to carry the total seismic mass of the structure; each perimeter frame was assigned to carry half the building seismic mass with masses lumped at floor levels. With the simplification to a 2D analysis, corner column effects due to bi-directional horizontal ground motion are not captured.

The structural analysis model of the building was developed to account for both non-linear geometry (P-Delta effect) and non-linear material properties. It consists of an assemblage of line elements representing the flexibilities of beams and columns. These line elements are connected to zero-length joints. The frame was assumed to have fixed supports at the foundation. The diaphragm was assumed rigid; all the joints at a given level were constrained to have equal horizontal displacements. For dynamic analyses, damping was assumed equal to 2% of the critical damping. To model the non-linear flexural behavior of the structure, a lumped plasticity approach was used for both beams and column. By this approach, all the elements consist of three parts: a linear elastic element and two rotational springs, one at each end. The linear elastic elements have flexural stiffness properties calculated from the members' cross section characteristics. These stiffnesses were reduced in accordance with ASCE-41 Supplement 1 (2006) stiffness modification factors to account for concrete cracking and reinforcement slip from connections. The rotational spring element behavior was simulated based on the Clough model, using hysteresis implemented in OpenSees by Ibarra et al. (2005). The most important aspect of this model is the postcapping negative slope, which enables modeling of the strain-softening behavior associated with concrete crushing, reinforcement buckling, and reinforcement fracture. The model also incorporates cyclic strength degradation. The parametric values for the calibration of the spring elements were calculated according to the equations presented in Haselton et al. (2007). These equations were also shown by Galanis et al. (2014) to represent with sufficient accuracy the dynamic collapse performance of concrete frames. More details about the structural model can be found in ATC 78-2 (FEMA; 2014) and in Galanis and Moehle (2012).

The periods of the first three modes of the modeled structure are listed in Table 1.

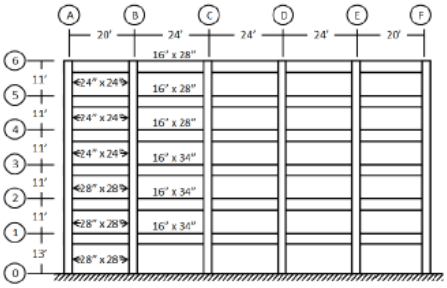

Figure 2: Elevation view of the perimeter frame

Table 1: First three modes of the studied building

Modes	Modal Period (sec)
1st	1.37
2nd	0.48
3rd	0.28

4. NEAR-FAULT GROUND MOTION DATASETS

This section describes the suites of recorded and synthetic near-fault ground motions that the studied building is subjected to. The recorded motions are selected based on FEMA P695 (2009); the synthetic motions are generated using the parameterized stochastic model of pulse-like and non-pulse-like near-fault ground motions in two orthogonal horizontal directions (Dabaghi and Der Kiureghian, 2014).

4.1. Dataset of recorded pulse-like near-fault ground motions

FEMA- P695 (2009) recommends a methodology, and provides two specific sets of ground motion records, a far-field set and a near-fault set, for the collapse assessment of buildings using non-linear dynamic analysis. These record sets were selected from the PEER NGA database, an earlier version of the NGA-West2 database (http://peer.berkeley.edu/ngawest2/). These sets only include records that satisfy a specified set of criteria; e.g., they must be strong-motion records (with $PGA > 0.2$ g and $PGV > 15$ cm/sec) from large-magnitude ($\mathbf{M} > 6.5$) shallow crustal earthquakes (strike-slip or reverse), and must be recorded at soft rock or stiff soil sites. The difference between the far-field and near-fault sets lies in the source-to-site distance criterion; a record is near-fault if it is recorded at a distance less than 10 km from the

fault rupture plane. A complete description and explanation of the selection criteria can be found in the FEMA P695 report (2009).

In this paper, the building of interest is assumed located in a region near active faults; only the near-fault record set of FEMA P695 is considered. This set consists of 28 records all recorded at a distance less than 10 km from the fault rupture plane, and each providing two horizontal components: in the fault-normal (FN) and fault-parallel (FP) directions. In FEMA P695, 14 of these records were classified as pulse-like and 14 as non-pulse-like based on the first version of the wavelet classification procedure proposed by Baker (2007a).

In this study, a subset of the FEMA P695 near-fault record set is used with slight modifications in the classification procedure and in the horizontal components. The subset is obtained as follows: (1) only 19 out of the 28 FEMA P695 near-fault records are considered, because their data was readily available; (2) these 19 records are classified as pulse- and non-pulse-like using the more recent wavelet classification procedure by Shahi and Baker (2011); (3) only the 14 records classified as pulse-like are included; (4) their horizontal components are rotated into the direction containing the largest pulse (denoted PP) and the corresponding orthogonal direction (denoted PO); see Shahi and Baker, 2011, and Dabaghi and Der Kiureghian, 2014. The resulting pulse-like near-fault records used in this study, their information, and their classification are listed in Table 2. The study will later be extended to the records classified as non-pulse-like.

4.2. Dataset of simulated pulse-like near-fault ground motions

To generate synthetic near-fault ground motions, the parameterized stochastic model of near-fault ground motions and the simulation procedure developed by Dabaghi and Der Kiureghian (2014) are used. These model and procedure were adapted and extended from the model and simulation procedure developed for far-field ground motions by Rezaeian and Der Kiureghian (2010, 2012). The model of near-fault ground motion considers both pulse-like and non-pulse-like ground motions. It is formulated in two orthogonal horizontal directions and in terms of physically meaningful parameters, which include measures of the intensity, duration, and frequency content of the ground motion. The model is able to represent the characteristics of recorded near-fault ground motions, including temporal and spectral non-stationarity, and the near-fault directivity effect. As described in Dabaghi and Der Kiureghian (2014), a preliminary model of the fling step may also be included but this feature is not used in this study.

Table 2: List of ground motion records used in this study; all are pulse-like near-fault ground motions.

NGA#	EQ Name	Year	Station Name	Pulse-like in FEMA P695?	T_p (sec)
181	Imp. Valley-06	1979	El Centro Array #6	Y	3.7
182	Imp. Valley-06	1979	El Centro Array #7	Y	3.5
723	Supers.Hills-02	1987	Parachute Test Site	Y	2.0
802	Loma Prieta	1989	Saratoga - Aloha Ave	Y	4.4
828	Cape Mendocino	1992	Petrolia	Y	2.8
879	Landers	1992	Lucerne	Y	5.3
1004	Northridge-01	1994	LA – Sep. VA Hos.	N	0.9
1063	Northridge-01	1994	Rinaldi Receiving	Y	1.2
1086	Northridge-01	1994	Sylm.OliveViewMedFF	Y	2.0
1165	Kocaeli, Turkey	1999	Izmit	Y	4.6
1176	Kocaeli, Turkey	1999	Yarimca	N	4.5
1503	Chi-Chi, Taiwan	1999	TCU065	Y	5.0
1529	Chi-Chi, Taiwan	1999	TCU102	Y	8.0
2114	Denali, Alaska	2002	TAPS P.Stat#10	N	2.8

Here, only the model of pulse-like ground motion is used. This model is formulated in the direction containing the largest pulse (denoted PP) and the corresponding orthogonal direction (denoted PO). The 19 parameters of the pulse-like model are identified by fitting to the time series characteristics of each of the target recorded pulse-like ground motions in Table 2. The fitted characteristics include the cumulative Arias intensity (i.e., the Husid plot), the cumulative number of zero-level up-crossings, and the rate of positive minima and negative maxima of the target recorded acceleration time series. Additionally for the PP component, parameters describing the amplitude and shape of

the pulse are fitted to the extracted pulse velocity time series. The ground motions in Table 2 were already fitted by Dabaghi and Der Kiureghian (2014); the details and results of the fitting procedure can be found there. Table 2 only reports the fitted values of parameter T_p, which denotes the period in seconds of the forward directivity pulse.

Using the simulation procedure proposed by Dabaghi and Der Kiureghian (2014), 10 synthetic motions are generated for each recorded motion using the corresponding fitted model parameters. Figure 3 shows the time series of the PP and PO horizontal components of record NGA#182, alongside one of its corresponding simulated ground motions. The figure illustrates the overall good agreement in the amplitude, duration, and frequency content of the recorded and synthetic ground motions, as well as in the forward directivity pulse observed in the velocity time series of the PP component.

Figure 4 shows the 2% damped pseudo-acceleration response spectra of the PP and PO components of each of the recorded ground motions of Table 2, and of their 10 simulated counterparts. Again, overall good agreement is observed: the response spectrum of a recorded ground motion component generally falls within the range spanned by the spectra of its simulated counterparts. Each recorded motion and its 10 corresponding synthetic motions may be regarded as different possible realizations of the modulated and filtered white-noise process from the same earthquake and for the same fitted parameters. However in a few cases (e.g., both the PP and PO components of NGA#828), the recorded and simulated spectra show differences at periods around 1 second. This is due to the idealized nature of the ground motion model, which with a small number of parameters cannot reproduce all the details of the recorded motion.

Figure 5 shows the median and median plus and minus two standard deviation levels for each of the 14 recorded and 14×10 simulated motions. The median spectra of both PP and PO components of the simulated dataset are similar

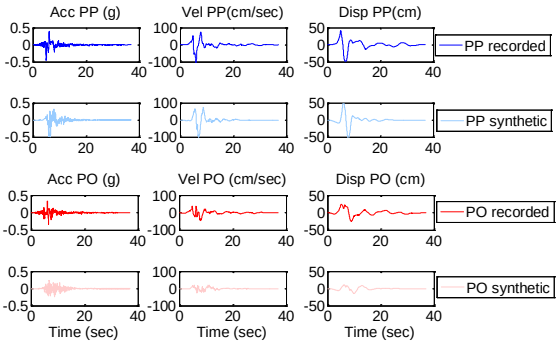

Figure 3: Acceleration, velocity and displacement time series of recorded (dark) pulselike near-fault ground motion NGA#182, and of a simulated motion (light) with parameters identified for record NGA#182; PP (blue) and PO (red) components.

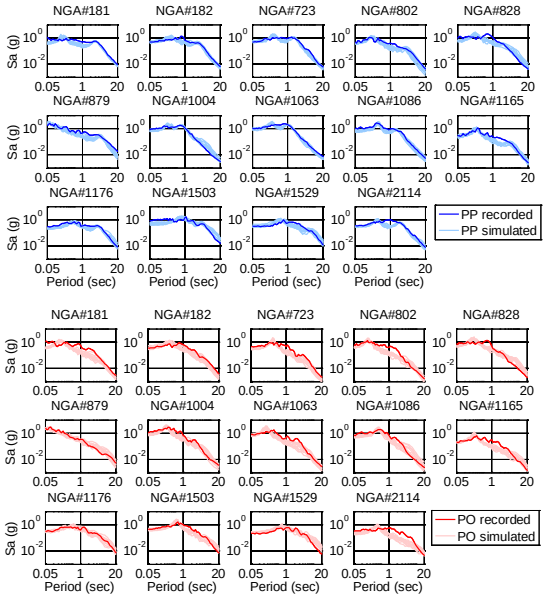

Figure 4: 2% damped pseudo-acceleration response spectra of PP (blue) and PO (red) components of each recorded (dark) and 10 corresponding synthetic (light) pulse-like near-fault ground motions

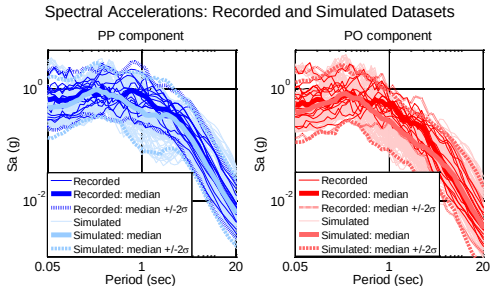

Figure 5: 2% damped pseudo-acceleration response spectra of PP (blue) and PO (red) components of all recorded (dark) and simulated (light) motions.

to those of the recorded dataset at periods shorter than about 0.8 sec and larger than about 3 sec. At periods between 0.8 and 3 sec, the simulated spectra tend to fall below their recorded counterparts.

5. ASSESMENT OF SEISMIC BEHAVIOR

IDA is used to assess the collapse performance of the studied 6-story building. According to this method, the non-linear response history analysis of a building model is performed for multiple individual ground motions, each gradually scaled to increasing acceleration amplitudes until the building reaches collapse (Vamvatsikos and Cornell, 2002). This study considers only sideway collapse, defined as maximum interstory drift ratio (IDR) exceeding 10% of story-height.

The recorded and synthetic suites of 14 pairs of pulse-like near-fault ground motions presented in the previous section are used. Each of these ground motions is gradually scaled, and the spectral acceleration level at the fundamental building period ($T_1 = 1.37$ sec) and leading to building collapse is measured. As mentioned earlier, it is not common to perform IDA using simulated motions, but this study uses IDA to explore differences in the responses of structures to recorded and simulated motions.

Figure 6 shows the IDA curves for the two horizontal components of record NGA#723 and of the 10 synthetic motions corresponding to record NGA#723 (i.e. simulated with the parameters identified for record NGA#723). Each point represents the result of one non-linear dynamic analysis of the studied building subjected to one ground motion component that is scaled to one intensity level. Each curve corresponds to one ground motion component; the differences between the curves reflect the differences in the duration and frequency content of the different ground motion components (FEMA, 2009). In Figure 6, it is observed that the IDA curves of the recorded components generally fall within the range of the IDA curves of their corresponding simulated motions. Moreover, the median collapse levels (i.e., at IDR=0.1) from the simulated motions are comparable to those from the recorded motions, for both the PP and PO components. This provides some confidence in the use of simulated motions as "realistic" realizations of real ground motions.

Figure 7 shows the IDA curves obtained using all recorded ground motions (left) and using the simulated motions corresponding to the recorded ones (right). Hereafter, only two out of the ten motions simulated for each record are used. Figure 7 suggests that the building response (IDA curves) to simulated motions is comparable to but presents a slightly larger variability than for recorded motions. At the onset of building collapse (at IDR=0.1), the corresponding spectral acceleration has a standard deviation of about 0.38 g for recorded motions and 0.50 g for simulated motions.

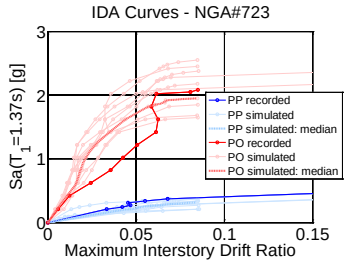

Figure 6: Comparison of IDA curves of recorded and simulated ground motions: record NGA#723 (dark), its 10 corresponding simulated motions (light), and median of the 10 simulated motions (dashed); PP (blue) and PO (red) horizontal components.

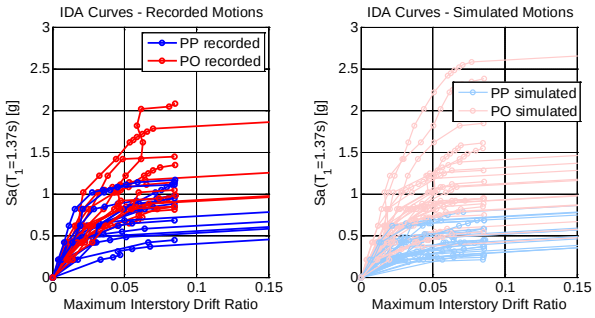

Figure 7: IDA curves for recorded (left, dark) and corresponding simulated (right, light) motions; PP (blue) and PO (red) horizontal components.

Figures 6 and 7 illustrate that the PP components of both recorded and simulated motions tend to cause collapse at lower intensity

levels than the PO components. This agrees with the common observation that pulselike near-fault ground motions are most damaging in the direction containing the largest forward directivity pulse (PP), a direction often close to the fault-normal direction.

6. RESULTS

A collapse fragility curve is defined as the cumulative distribution function (CDF) relating the probability of collapse to the ground motion intensity $S_a(T_1)$ (Ibarra et al., 2005). It reflects the record-to-record (RTR) variability in the ground motion intensity that causes collapse of a building. RTR variability arises from variability in the duration and frequency content of the individual motions.

Using the IDA results at the collapse threshold (IDR=0.1), empirical collapse fragility curves are obtained for the studied building with each of the recorded and simulated datasets; they are shown in Figure 8 alongside the lognormal distributions that are fitted without accounting for additional modeling uncertainty. The fragility curves from the simulated dataset fall slightly to the left of those from the recorded dataset. The median collapse capacity (i.e., the spectral acceleration level corresponding to a 50% probability of collapse) is $\hat{S}_{CT} = 0.89\,\mathrm{g}$ for the recorded dataset, and $\hat{S}_{CT} = 0.64\,\mathrm{g}$ for the simulated dataset. These results indicate that the duration and frequency content characteristics of the simulated ground motions are more damaging than those of the recorded ground motions. This can be explained by the observation that the simulated motions are less intense than their recorded counterparts near the first-mode period of the studied building (see Figure 5). Therefore, scaling the two sets to a common $Sa(T_1)$ results in the simulated ground motions being more intense at periods other than T_1. This study will later be extended to a building having a longer first-mode period, at which the recorded and simulated ground motion levels are more comparable. As in Figure 7, Figure 8 also illustrates the larger variability of the building response to simulated compared to recorded motions, with collapse capacity standard deviation values $\sigma_{\ln Sa(T_1)}$ of 0.6 and 0.4 for the simulated and recorded datasets, respectively.

Note that in earlier studies by Galanis and Moehle (2012) and in ATC 78-2 (FEMA, 2014), the collapse fragility curve was developed for the same 6-story building but for the dataset of far-field ground motion records of FEMA P695 (2009). In that study, the median collapse capacity was $\hat{S}_{CT} = 0.99\,\mathrm{g}$. This indicates that the dataset of recorded pulse-like near-fault ground motions used in this study is more damaging to the studied 6-story building than the FEMA P695 dataset of far-field ground motions.

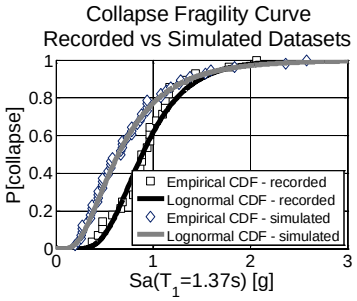

Figure 8: Collapse fragility curves obtained from recorded (black) and simulated (grey) ground motion datasets: empirical CDFs (squares and lozenges) and fitted lognormal distributions (solid lines).

7. CONCLUSIONS

In this paper, IDA and collapse performance assessment is performed for a 6-story reinforced concrete building and for two sets of pulse-like near-fault ground motions: (1) a recorded dataset based on FEMA P695 (2009); and (2) a synthetic dataset corresponding to the recorded one and generated using the parameterized stochastic model of near-fault ground motion by Dabaghi and Der Kiureghian (2014). The collapse assessment results from the two datasets are compared.

The major findings of this study for the investigated building are summarized as follows: (1) the component of a pulse-like near-fault ground motion that contains the largest directivity pulse tends to be more damaging than the corresponding orthogonal horizontal

component; (2) the considered pulse-like near-fault ground motions are more damaging than far-field ground motions used in FEMA P695; (3) the simulated motions used in this study are more damaging than their recorded counterparts; using the simulated dataset tends to underestimate the collapse capacity of the studied building. This may be due to the idealized nature of the model used to generate the synthetic motions. This model cannot reproduce all the details of the recorded ground motion and fails to capture the recorded ground motion intensities at periods near the first-mode period of the studied building.

In the next stages, this study will be continued at several levels: (1) the comparison between recorded and simulated motions will be extended to non-pulse-like near-fault ground motions and far-field ground motions; (2) other buildings will be investigated; e.g., buildings having a first-mode period at which the recorded and simulated motions are in better agreement, and older non-ductile buildings; (3) simulated motions will be used in a cloud analysis.

8. REFERENCES

ASCE, (2006), "Seismic Rehabilitation of Existing Buildings", ASCE/SEI 41-06, American Society of Civil Engineers.

Baker, J.W. (2007a). "Quantitative classification of near-fault ground motions using wavelet analysis." Bull. Seismol. Soc. Am., 97(5), 1486-1501.

Baker, J.W., (2007b), "Probabilistic Structural Response Assessment Using Vector-Valued Intensity Measures", Earthquake Engineering and Structural Dynamics, 36, 1861-1883.

Dabaghi, M., Der Kiureghian, A. (2014). "Stochastic modeling and simulation of near-fault ground motions for performance-based earthquake engineering." PEER Report No. 2014/20, University of California, Berkeley, CA.

Federal Emergency Management Agency (FEMA) (2009). "Recommended Methodology for Quantification of Building System Performance and Response Parameters." FEMA P695, Applied Technology Council.

Federal Emergency Management Agency (FEMA) (2013). "Evaluation of the Methodology to Select and Prioritize Collapse Indicators in Older Concrete Buildings." ATC 78-1, Applied Technology Council.

Federal Emergency Management Agency (FEMA) (2014). "Seismic Evaluation for Collapse Potential of Older Concrete Frame Buildings." ATC 78-2, Applied Technology Council.

Galanis P., Shin Y.P., and Moehle, J.P., (2014), "Modeling the Dynamic Structural Behavior of Ductile and Non-Ductile Reinforced Concrete Frames", 10th NCEE, July 21-25 2014, Alaska.

Galanis, P.H., Moehle, J. P. (2012). "Development of Collapse Indicators for Older-Type Reinforced Concrete Buildings",15WCEE,Lisbon,Portugal

Galanis, P.H., Moehle, J. P. (2014). "Development of Collapse Indicators for Risk Assessment of Older-Type Reinforced Concrete Buildings". Earthquake Spectra (online preprint).

Haselton, C.B., Liel, A.B., Taylor-Lange, S., Deierlein G.G.(2007). "Beam-Column Element Model Calibrated for Predicting Flexural Response Leading to Global Collapse of RC Frame Buildings." PEER Report No. 2007/03, University of California, Berkeley, CA.

Ibarra, L.F., Medina, R.A., and Krawinkler, H. (2005). "Hysteretic models that incorporate strength and stiffness deterioration," Earthq. Eng. Struct. Dyn., 34(12), 1489-1511.

Rezaeian, S., Der Kiureghian A. (2010). "Simulation of synthetic ground motions for specified earthquake and site characteristics." Earthq. Eng. Struct. Dyn., 39, 1155–1180.

Rezaeian, S., Der Kiureghian, A. (2012). "Simulation of orthogonal horizontal ground motion components for specified earthquake and site characteristics." Earthquake Engineering & Structural Dynamics, 41, 335–353.

Shahi S.K., Baker J.W. (2011). An empirically calibrated framework for including the effects of near-fault directivity in probabilistic seismic hazard analysis, Bull. Seismol. Soc. Am., 101(2), 742–755.

Somerville P.G., Smith NF, Graves R.W., Abrahamson N.A. (1997). "Modification of empirical strong ground motion attenuation relations to include the amplitude and duration effects of rupture directivity", Seism. Res. Lett., 68: 94-127.

Vamvatsikos, D., Cornell, A.C. (2002) "Incremental Dynamic Analysis." Earthquake Engineering and Structural Dynamics, 31, 491-514.